

# **Characterization of a Superconducting nanowire single photon detector**

**Max Reicherd**

Bachelorarbeit in Physik  
angefertigt im Institut für Angewandte Physik

vorgelegt der  
Mathematisch-Naturwissenschaftlichen Fakultät  
der  
Rheinischen Friedrich-Wilhelms-Universität  
Bonn

Juli 2024

I hereby declare that this thesis was formulated by myself and that no sources or tools other than those cited were used.

Bonn, .....  
Date .....  
Signature

1. Reviewer: Prof. Dr. Sebastian Hofferberth
2. Reviewer: Prof. Dr. Daqing Wang

---

## Acknowledgements

---

I would like to thank ...

You should probably use \chapter\* for acknowledgements at the beginning of a thesis and \chapter for the end.

---

# Contents

---

<b>1</b>	<b>Introduction</b>	<b>1</b>
<b>2</b>	<b>Working principle of SNSPDs</b>	<b>2</b>
<b>3</b>	<b>Faint laser source for detector characterization</b>	<b>5</b>
3.1	Characteristics of faint laser sources . . . . .	5
3.2	Experimental setup . . . . .	6
<b>4</b>	<b>Characterization of a SNSPD by Single Quantum</b>	<b>9</b>
4.1	Dark Count Rate . . . . .	9
4.2	Recovery time . . . . .	11
4.3	Efficiency . . . . .	15
4.4	Discussion . . . . .	19
<b>5</b>	<b>Conclusion and Outlook</b>	<b>20</b>
<b>A</b>	<b>Appendix</b>	<b>21</b>
A.1	ND filter calibration . . . . .	21
A.2	Recovery time measurements . . . . .	22
A.2.1	Recovery time measurements - Oscillating bias current . . . . .	22
	<b>Bibliography</b>	<b>23</b>

# CHAPTER 1

---

## Introduction

---

## CHAPTER 2

---

### Working principle of SNSPDs

---

This chapter will introduce the working principle of superconducting nanowire single photon detectors (SNSPDs). 1-2 sentences to history for introduction Wikipedia provides good stuff for introduction Here only phenomenological explanations is given. More details can be found in ..

The SNSPD has four parts, as shown in figure 2.1. The central detection area is made of a superconducting nanowire on a sapphire base. The superconducting nanowire is made of a thin film of a superconducting material, like niobium nitride (NbN). The sapphire layer is used to dissipate the heat when the wire heats up. Further, a gold contact supplies a bias current through the superconducting nanowire and an optical fibre is coupled to the detection area.

To operate the system, the setup is cooled below the critical temperature of the superconductor to 2-3K and a DC current is applied to the nanowire.

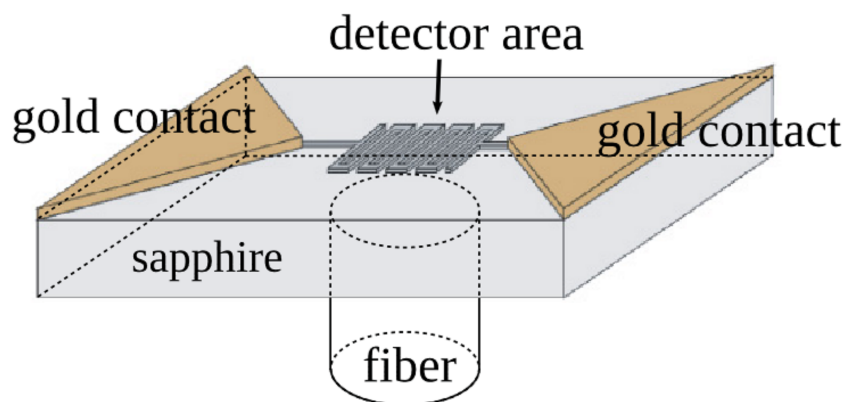


Figure 2.1: (a) Schematic structure of a superconducting nanowire single photon detector [1]

The detection process is shown in the figure 2.2.

Photons hit the superconducting nanowire (ii) and break up individual Cooper pairs. This leads to a local reduction of the critical current below the bias current and in turn to a localised area where the superconductivity is interrupted, this local area forms the so-called "hotspot" (iii). This hotspot forms

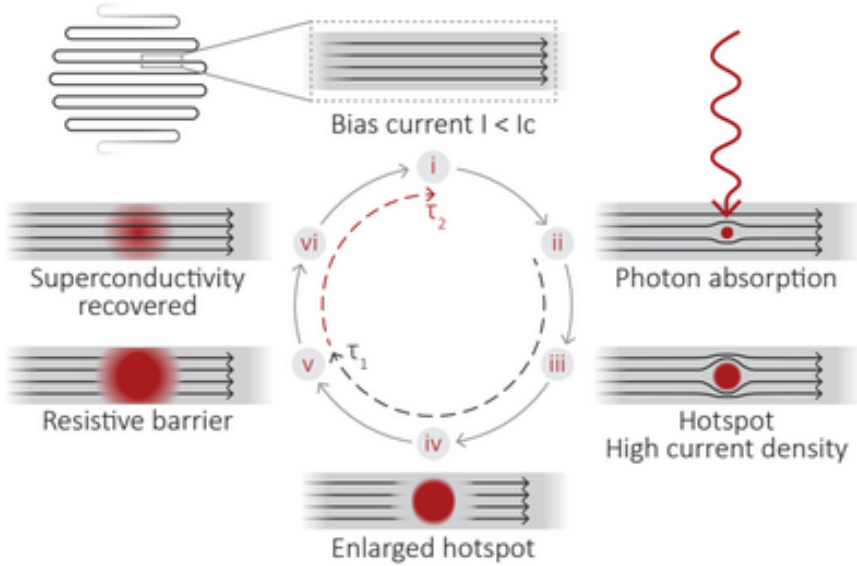


Figure 2.2: Schematic detection cycle of a superconducting nanowire single photon detector [2]

a resistance area because the critical temperature is exceeded by the energy of the photon. In response, the current flows around this hotspot (iv), whereby the local current density in the side areas next to the hotspot again exceeds the critical current, due to a higher current density. If the critical current is exceeded, the superconductivity also breaks down in these areas. This excess also causes a resistance in the side channels of the nanowire (v). Ultimately, this rapid increase in resistance can be measured in form of a voltage pulse. The local non-superconducting area is then cooled down by the cryogenic environment and returns to the superconducting state (iv—i).

One important technical detail is the fiber coupling of this detector because the efficiency and timing jitter depend on it. Depending on in which polarization the light hits the meander, the efficiency changes. When light hits the wire orthogonally polarized to the wire direction, the photon is less efficiently absorbed, than polarized parallel to the wire.

As seen in fig. 2.3 the coupled fibre in our characterized detector is parallel polarized to the nanowire. Moreover, to cover the whole light, shined out of the fibre, the geometry of the detection zone is constructed as a round plate and has roughly the same diameter as the fibre output (FC/PC). A smaller area would risk not absorbing each photon and a larger area would increase the time leading the signal to the computer unit.

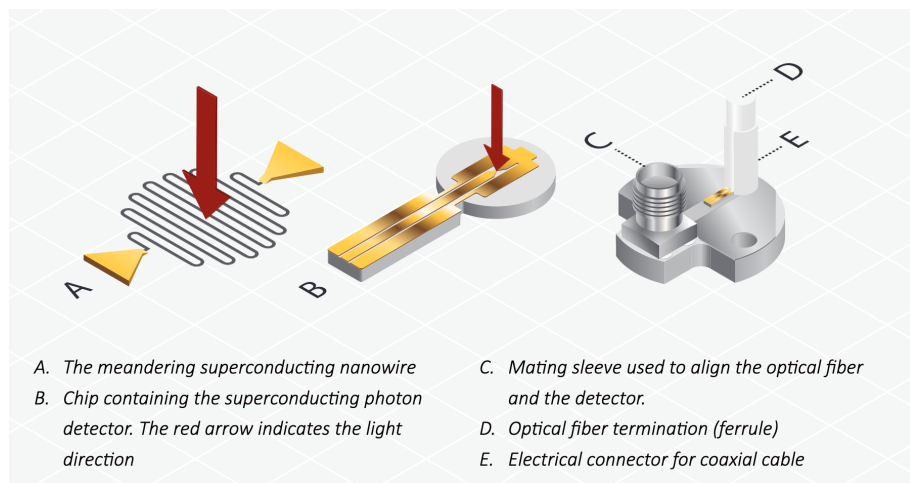


Figure 2.3: Scematic set up of the fiber coupling of a superconducting nanowire single photon detector [Zitieren!](#)

# CHAPTER 3

---

## Faint laser source for detector characterization

---

Counting photons one has to consider not only the characteristics of the detector but from the emitter source as well. The section focus is the characteristics of the laser setup serving as a light source for the detector characterization. For this, I briefly sum up characteristics of a coherent laser light source and its conditions it gives for detector characterization. Furthermore, I introduce the setup I build for characterizing the SNSPD.

### 3.1 Characteristics of faint laser sources

Using a laser source enables us considering the emitting light as monochromatic beam with angular frequency  $\omega$  and constant Intensity  $I$ . The Photon flux of a laser is defined as the photon average number passing through a cross-section in one unit time:

$$\Phi = \frac{IA}{\hbar\omega} = \frac{P}{\hbar\omega} \text{photons } s^{-1} \quad (3.1)$$

where  $I$  is the current of photon,  $A$  the cross-section,  $P$  the laser power and  $\omega = \frac{2\pi c}{\lambda}$  the angular frequency which depends on the wavelength. The average number of registered counts  $N(T)$  for a given detection time  $T$  by a detector is given by:

$$N(T) = T\Phi\eta = \frac{PT\eta}{\hbar\omega} \text{photons} \quad (3.2)$$

and hence the registered counts  $\mathcal{R}$  per unit time is described by:

$$\mathcal{R} = \frac{N(T)}{T} = \eta\Phi = \frac{P\eta}{\hbar\omega} \text{photons } s^{-1} \quad (3.3)$$

where  $\eta$  is the efficiency of the detector system which is described in more detail in section 4.3.

The detector has a maximal detection count rate, and it is restricted by the recovery time 4.2 of the detector  $\mathcal{R}_{\max} \propto \frac{1}{\tau_r}$ . When sending to many photons at the same time to the detector latching appears

[3] and counting in this state is not possible. Therefore, the photon rate send to the detector has to be below the maximal detection count rate of the detector. As consequence for this experiment, the laser power has to be attenuated to a level where the photon rate is below the maximal detection count rate of the detector.

The photon statistic of coherent light, in our case (in reasonable approximation) of our laser light, is given by poisson statistics. This characteristic stems from discrete nature of photons, hence photons are random distributed with non-equidistant spacing between each other.

Considering the fact, that the detector is not able to detect photons within the deadtime and with significant lower efficiency in the reset time, one has to look at the probability of photons in those blind spots to include this in later evaluation.

The amount of photons is calculated by looking at the probability measuring one photon per length segment, given by the deadtime and the reset time. First, we consider one Length segment given by the deadtime  $\tau_d$ , the reset time  $\tau_{\text{res}}$  and the measurement time  $\tau_m$ :

$$L_d = c\tau_d \quad (3.4)$$

$$L_{\text{res}} = c\tau_{\text{res}} \quad (3.5)$$

$$L_m = c\tau_m \quad (3.6)$$

With this, we can calculate for a given measurement time the average photon rate  $\bar{n}$  per length segment  $L_m$

$$\bar{n} = \Phi \frac{L_m}{c} \quad (3.7)$$

$$(3.8)$$

and further the probability of finding one photon in the particular line segment  $L_d$ :

$$p = \frac{\bar{n}}{N} \quad (3.9)$$

Where  $N = \frac{c}{L_d}$  are the subsegments of the measured length segment  $L_m$ .

This enables us to calculate the probability  $p_{\text{dead}}$  of finding n Photons per deadtime segment  $L_d$  and  $p_{\text{res}}$  per reset time segment. This probability yields the amount of photons we inherently can not measure due to the detector limitations, hence include this results in calculating the efficiency of the SNSPD.

### 3.2 Experimental setup

From factory details it is known that the recovery time of the detector is located between 17 and 23ns, depending on the detector settings. This details can be confirmed by our measurements as well 4.2. This gives a theoretical maximum detection rate with constant maximal possible efficiency of  $\mathcal{R}_{\max} \propto \frac{1}{\tau_d} \approx 43 - 58\text{MHz}$ . However, this rate would only hold, if the emitter would be a true single photon source with a consistent emitting rate, where photons are equidistantly spaced. Since we use a

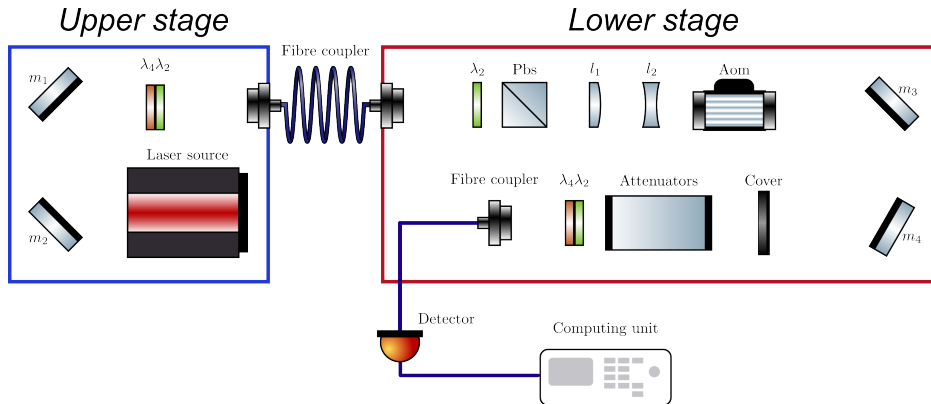


Figure 3.1: Set up for attenuation of a 780nm laser source from the Russian company [Vitawave](#)

coherent laser source the counting rate is significantly lower than the theoretical maximum detection rate. From the factory we got specification of about 2-4 MHz as detection count rate with maximal detection efficiency [Source](#).

The initial situation is that the minimum laser power of the laser source is higher than the maximal detection count rate of the detector. The reason for this is that the laser source does only lase with a constant power with a certain minimum power. Therefore, the laser power can not be regulated down by adjusting the input power of the laser, but has to be attenuated by neutral density filters afterwards.

In order to realize the laser attenuation the setup shown in fig 3.1 was build. The first coupling of the laser light at the upper stage was done in order to operate with the beam on the lower stage, because the laserbeam was due to its construction on an uplifted stage. Afterwards, on the lower stage the beam passes a half-wave plate  $\lambda_2$  and polarization beam splitter (pbs) to filter the horizontal polarized E-field out. Further, a galilei telescope was build ( $l_1$  and  $l_2$ ) out of one focal and one diffusing lens for reducing the beam width, so it fits fully on the surface of the crystal of the Acousto-optic modulator (AOM). The first order of the AOM was used for flexible voltage modulation of the laser. A cover was used to filter out the first from the zeroth order of the AOM. Then a flip mount was placed, where Neutral density (ND) filters could be placed in and flexible placed in and out of the laser beam. The ND filters have the function to attenuate the laser light. At the end, before the laser light was again coupled in, again a half-wave plate  $\lambda_2$  and quarter-wave plate  $\lambda_4$  were used to stabilize and control the light polarization coupling in the fibre. As mentioned in 2 the light was polarized according to the slow axis of the fibre. Afterwards the light was coupled back into a fibre, so it was directed to the detector. Technically, it was important coupling to a APC/PC to FC/PC optical fibre because the detector only had an FC/PC optical fibre input port, in order to maintain higher efficiency coupling in the light [3].

Besides, this optical setup had to be protected from environmental light. For this, the room where the setup was running was shielded with alu foil which has a reflection coefficient of almost 90% at the operating wavelength of 780nm [Source](#). Moreover, a black box was build. It has the function to avoid further environmental light coupling into the fibre. Additionally, the optical fibre running from the optical setup to the detector was shielded with alu foil as well to avoid absorption from the optical fibre.

Based on those theoretical considerations and our experimental setup, one can approach the central goal to determine the amount of photons and with this, determine the efficiency of the detector.

Central, in order to do efficiency measurements, on the one hand one must send only a few photons (low power) and one must exactly know how many photons are sent. For this we need to measure the power of the laser light, we are sending to the detector. However, the desired light is so weak, we cannot measure it with power-meters or any other measurement devices available to us. So our photon rate we are expecting to send to the detector depends on the ND filters and their optical density (OD) value, since it is the sole factor we can adjust our laser power (here transmission)( $T = 10^{-OD}$ ), hence our amount of photons we send to the detector.

The challenge relying on ND filters is that the fabric values of their OD are not precise, hence the filters need to be calibrated by oneself and as precise as possible, to get accurate and stable OD values for the ND filters.

To get accurate results, the OD value of each filter is measured with two methods to reduce systematic errors. The first method measures the OD values, where the ND filters are set in the flip mount as shown in graph 3.1. The second method measures the OD values after the fibre coupling directly in front of the powermeter outside the blackbox to avoid straying light from the elements in the setup.

The attenuation of ND filters is quantized via the OD value and is connected to the transmission value  $T = 10^{(OD)}$  of the outgoing light. Due to the logarithmic definition of the OD value, the OD values of the ND filters are added up when they are stacked on each other.

The measurement of the OD values was done by sending light on the filter and measuring the power with and without the filter. Moreover, only single ND filter measurements were in the measurable range, since the powermeter was not able to measure the power of the attenuated laser light by several stacked ND filters.

The OD value is then calculated by the logarithmic value of the inverse transmission value  $\log_{10}(\frac{1}{T})$ . The transmission value is given by the proportion of the power with the filter compared without the filter  $T = \frac{P_{out}}{P_{in}}$ . Afterwards, the final OD values of each method were combined and the corresponding systematic and statistical errors are considered in order to get accurate OD values for the ND filters. Results of the measurements and error calculations can be found in section A.1.

Based on these OD values the photon rate was determined.

# CHAPTER 4

---

## Characterization of a SNSPD by Single Quantum

---

In literature, four central characteristics have emerged to quantify the quality of single photon detectors and make their performance comparable [4, 5]. These characteristics are the system detection efficiency  $\eta_{\text{sde}}$ , the dark count rate (DCR), the recovery time ( $\tau_{\text{recovery}} = \tau_{\text{rec}}$ ) and the timing jitter. In this thesis, I focus on the detector efficiency  $\eta_{\text{sde}}$ , the dark count rate (DCR) and the recovery time ( $\tau_{\text{rec}}$ ). In general there are more than these introduced figures of merits, like after-pulsing but these will not be considered in this thesis.

### 4.1 Dark Count Rate

The DCR is the rate of measured detection events not intentionally sent from the source (here the faint laser source). It is measured in counts per second and can be caused by statistical fluctuations in the measurement electronics. A low DCR is important for a high signal-to-noise ratio and means easy interpretable results which are not distorted by noise [6].

In the context of SNSPDs, the DCR is dependent on the bias current applied to the nanowire. This is due to the fact that if the bias current approaches the critical current, less current  $\Delta I = I_c - I_B$  is needed to exceed the critical current. Therefore, electronic fluctuation, close to the critical current will cause a breakdown of the superconducting state and hence a dark count more often. Furthermore, it is important to perform DCR measurements first in the characterization process because it determines the limit, where general measurements are not distorted by high DCR noise.

#### Measurement and results

In order to evaluate the DCR, it is necessary to perform measurements in two different setups. First, a setup in which no optical fibre is connected to the detector and the port is covered. In such a setup, it can be assumed that no photons from the surrounding environment are striking the detector. This allows for the measurement of the DCR only triggered by the electronics noise depending on the detector's bias current and trigger voltage.

The required measurement setup consists out of the detector with the protection cap on the output port of the detector. This configuration represents the most shielded environment from external light sources and serves as the reference value for optimal DCR values achievable in single photon

measurements. The measurement was conducted by sweeping the bias current from 0 to  $35\mu\text{A}$  in  $0.1\mu\text{A}$  increments with an integration time of 200ms at each step

The second setup involves connecting the detector to the faint laser source of section 3.1. The laser source was turned off, so no photons from the source were sent to the detector. This is done in order determine the DCR for consecutive measurements and improve the light shielding of the setup and the optical fibre. This allows one to find the optimal shielding configuration for the highest signal-to-noise ratio. Once more, the bias current was swept from 0 to  $35\mu\text{A}$  in  $0.1\mu\text{A}$  increments with an integration time of the count rates for 200 ms. In fig ?? the results are shown for an optimized and a non optimized case.

At the initial, non optimized configuration an optical fibre was connected to the detector's output port and the fibre output coupling of the experiment. The laser source was turned off, so only electronic fluctuations and ambient light hitting the detector can cause detection events. To reduce dark counts due to ambient light a black box was constructed that covers the laser setup. Further, the fiber was wrapped in aluminum foil to prevent ambient light to couple to the core through the cladding.

As expected, the DCR rise in each case in ?? with decreasing difference  $\Delta I = I_c - I_B$  due to raising probability that weak electronic noises trigger a signal. The orange curve in ?? demonstrates that in the absence of protection, a significant number of photons from the environment are able to enter the detector through various potential pathways like the fibre cladding or the coupling connection to the laser setup.

In contrast, the measurement results with full shielding, depicted in figure 4.1 as well, show, that the DCR of the coupled and protected setup is the same as to the DCR with a cap on. The peaks in the green curve at  $\approx 3$  and  $\approx 14\mu\text{A}$  are artifacts resulting from some leakages in the protection. Nevertheless, these leakages are not substantial when viewed in the context of the total photon count rate, particularly when considering the anticipated photon rates from the faint weak laser source operating in the high kHz and MHz frequency ranges.

Lastly, one can conclude from the investigation of the DCR of channel 1, that all further measurements have to be done at a bias current of  $I_B \approx 31.2\mu\text{A}$ . As mentioned above the final figure of merit for the DCR is depending on the bias current working point. In this work, five 60s measurements were done for three different bias currents ( $24$ ,  $28$  and  $31.2\mu\text{A}$ ).

The averaged results for channel one of the detector yield a DCR of:

$$DCR_{24\mu\text{A}} = (5 \pm 0.0001)\text{Hz} \quad (4.1)$$

$$DCR_{28\mu\text{A}} = (4 \pm 0.0001)\text{Hz} \quad (4.2)$$

$$DCR_{31.2\mu\text{A}} = (3 \pm 0.0001)\text{Hz} \quad (4.3)$$

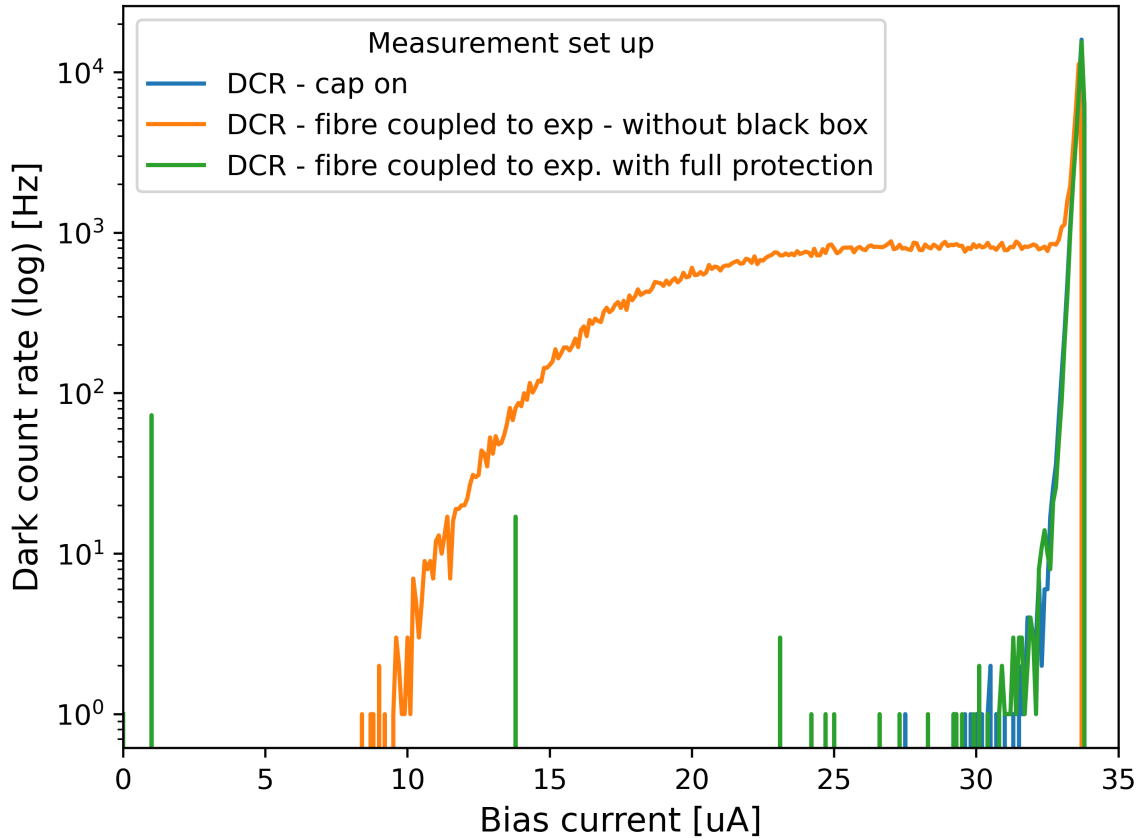


Figure 4.1: Channel 1 DCR measurements for different bias currents at a trigger voltage of 200MHz. The blue curve shows the DCR with a cap on the output port of the detector. The orange curve shows the DCR with a fibre connected to the detector and the fibre output coupling of the experiment. The green curve shows the DCR with a fibre connected to the detector, the fibre output coupling of the experiment and alumni foil wrapped around the optical fibre.

## 4.2 Recovery time

The concept of the recovery time is visually depicted in fig 4.2. When a photon hits the detector and is absorbed, the efficiency of the detector drops to zero and no further photons can be measured for a certain period of time. This elapsed time is called the dead time  $\tau_{\text{dead}} = \tau_d$ . The efficiency then rises again to the original device efficiency  $\eta_G$ . This period is called the reset time  $\tau_{\text{reset}} = \tau_r$ . The vertical dashed line forms the starting point where the efficiency rises again to the original device efficiency  $\eta_G$ . Finally, the sum  $\tau_{\text{rec}} = \tau_r + \tau_d$  of both times forms the recovery time  $\tau_{\text{rec}}$ .

The recovery time is important because it determines the rate the detector can detect photons. The lower the recovery time, as higher the counting rate.

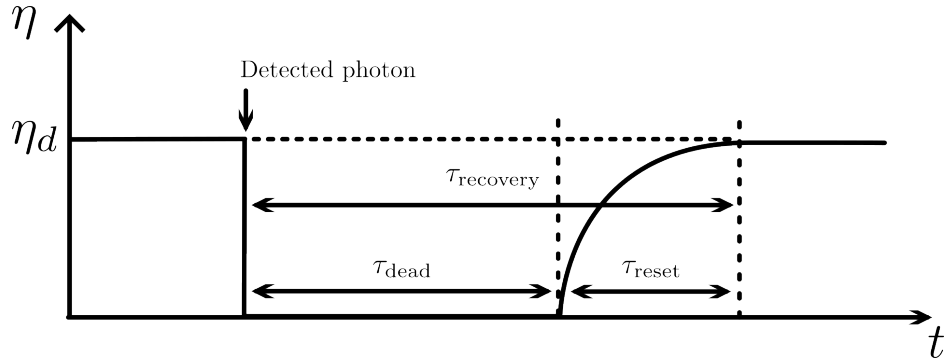


Figure 4.2: Schematic efficiency curve for the detection of a photon[7]. On the Y axis is the efficiency  $\eta$ , where  $\eta_G$  is the device efficiency. On the X axis is the time course of the efficiency. The trajectory of the initial device efficiency, represented by the variable  $\eta$ , does not align with the illustration

## Measurement and results

In this work, the recovery time of the detector is determined through an autocorrelation method based on a continuous wave laser source (a faint laser source), a technique that has been previously employed by other research groups. [8, 9]. The measurement was conducted with the setup shown in fig 4.3. The raw analog signals from the detector were directly transmitted to a time tagger unit (Time Tagger 20) by Swabian instruments. with self-adjustable trigger voltages, a device deadtime of 6ns and a maximal counting rate of 9MHz.

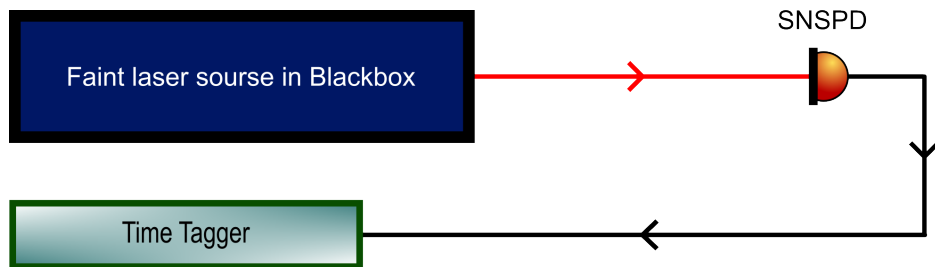


Figure 4.3: Experimental setup for measuring the recovery time. Optical setup of "faint laser source in black box" is depicted in 3.1

This unit enabled the tagging of incoming signals with a time tag, as implied by its name. Subsequently, the tags were used to process the time distances between all signals. The histogram of these distances provide an autocorrelation in time (here not normalized). The autocorrelation was measured for one channel for four different bias currents ( $26\mu\text{A}$ ,  $28\mu\text{A}$ ,  $31\mu\text{A}$  and  $31.2\mu\text{A}$ ) and trigger voltages ( $300\text{mV}$ ,  $400\text{mV}$ ,  $500\text{mV}$  and  $600\text{mV}$ ).

These measurements were done to determine the recovery time and analyze its dependencies. The results for a fixed bias current of  $31.2\mu\text{A}$  are shown in figure 4.4(a) and for  $26\mu\text{A}$  in 4.4(b). The other measurement results are presented in the appendix A.2.

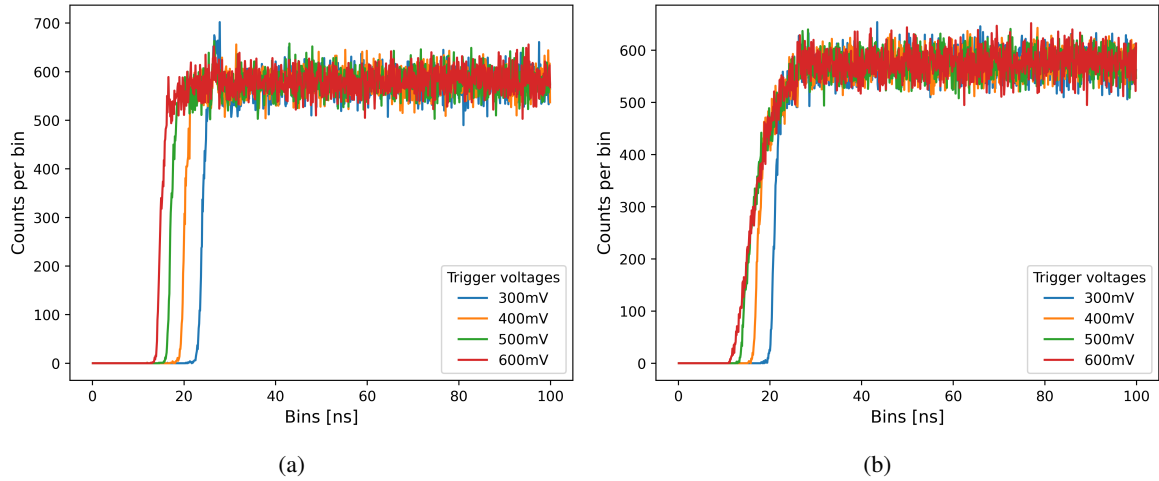


Figure 4.4: Autocorrelation of distances between two photon detection events for (a)  $I_B = 31.2\mu A$  and (b)  $I_B = 26\mu A$ . The X-axis represents the time distance between two signals in 1ns steps and the Y-axis the counts per bin.

The results of the autocorrelation show three major features. First, for low trigger voltages, the dead time is longer and decrease for increasing trigger voltages. This is true for both, the lower and higher bias current. The reason for this behavior can be explained best by looking at an exemplary raw analog signal (see fig 4.5) of two consequent pulses. In figure 4.5 one can see the peaks of two consecutive detection signals, where the second pulse starts ( $\approx 20\text{ns}$ ) before the falling edge of the first pulse ends. Physically, that means, that before the first signal spike has fully decayed a second photon, already hit the detector, got detected and produced a second spike.

If the trigger is below 500mV the time tagger will count this signal as one count, since the second pulse came when the remaining voltage of the wire was above 500mV. If the trigger is above 500mV both pulses will be counted. This allows successive events with smaller time delay between them and therefore reduces the perceived recovery time. However, only with a lower count rate which can be seen at the left rising edge in both figures 4.4. This is due to the fact that the detector is not fully recovered yet and counts are detected in the  $\tau_{\text{reset}}$  regime and therefore the detection efficiency is lower.

Secondly, for the lower bias current ( $26\mu A$ ), the rising count curves for each trigger voltage converge earlier in comparison to the bias current of  $31.2 \mu A$ . At the bias current of  $31.2 \mu A$ , the four different count curves remain distinct until they reach their peak. This can be attributed to the differing pulse heights, dependent on the bias current. According to Ohm's law, for the same resistivity, a lower bias current corresponds to lower voltage pulses and vice versa. Due to the lower pulse, the regime, where pulses can be resolved by a trigger voltage of 600mV but not 500mV becomes smaller. The different pulse heights can also be verified by the recorded analog signals shown in figure: ??.

The third interesting feature is the count peak at 24-27ns for  $31.2\mu A$  and a trigger level of 300 mV 4.4(a).

This small peak is less visible at lower bias currents or higher trigger levels. Closer examination of this trend are shown in the appendix A.

This behavior can be understood by taking into account that the bias current needs a finite amount of time to reach its target value once the superconductivity is restored and will also overshoot a bit after reaching the target value. A sketch of the expected behavior is shown in figure 4.6.

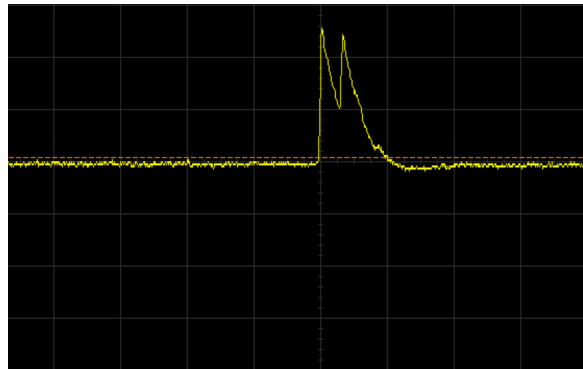


Figure 4.5: Analog signal screenshot of an oscilloscope from channel 1 for a bias current of  $31.2\mu\text{A}$  and a trigger of  $600\text{mV}$ . X-axis: time in  $50\text{ns}$  steps (straight vertical yellow lines), Y-axis voltage in  $500\text{mV}$  steps (straight horizontal yellow lines)

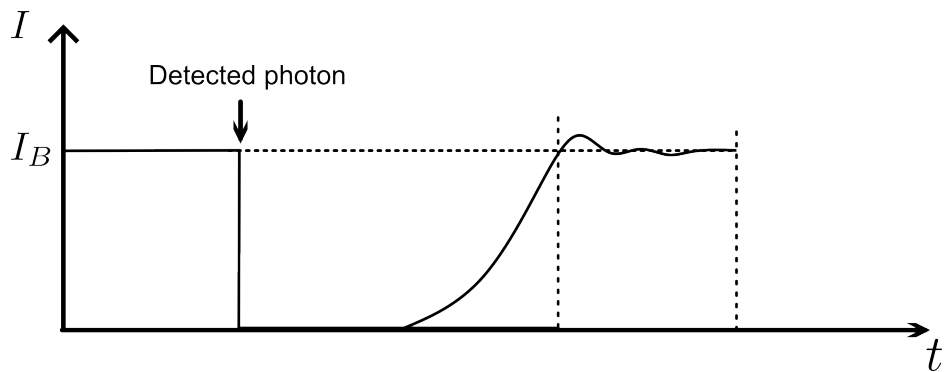


Figure 4.6: A sketch of the assumed bias current behaviour is presented herewith. Once the bias current has been reached, the current undergoes a brief oscillation before stabilising at the bias current level.

Following the detection of a current, the course of the current does not proceed directly and precisely to the bias current. Instead, it oscillates for a brief period and then rapidly reaches equilibrium.

If the target bias current is close to the critical current the overshooting might cause a breaking of the superconductivity leading to a time correlated increase in the dark current rate (seen in figure 4.1). This feature is less severe for higher trigger voltages which suggests that the self triggered pulse is typically of smaller height.

It can be concluded that the optimal recovery time is achieved when the detector is operated at a bias current maintained at a level that is close but not excessive to critical current of  $31.2\mu\text{A}$  and a trigger voltage of  $600\text{V}$ .

This enables the generation of a higher pulse, which in turn results in a steeper reset time, a shorter dead time, and consequently, a shorter recovery time.

**DISCLAIMER: ALL THE RESULTS AND METHODS ARE NOT FINALIZED AND WILL BE ADAPTED, IF METHOD IS AGREED**

Finally, a reasonable trigger point for a bias current of  $31.2\mu\text{A}$  is  $600\text{mV}$ , which yields the lowest recovery time. The calculation of the  $\tau_{\text{rec}}$  is done, by calculating the average of counts per bin from  $30\mu\text{A}$  till the end of the measurement period. Here, I choose  $30\mu\text{A}$  as the starting point, because from

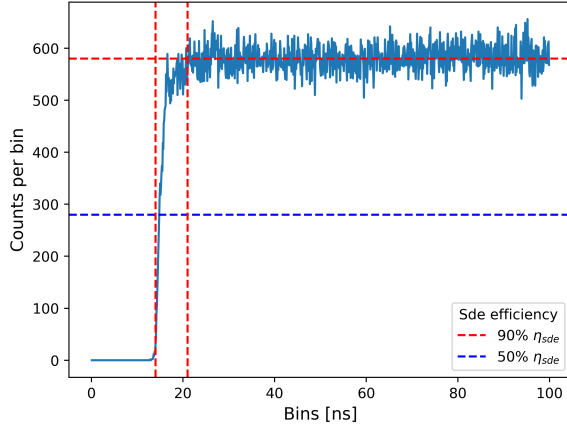


Figure 4.7: Histogram of distances between signals for  $I_B = 31.2\mu A$  and 600mV. H- and v-lines indicate the dead-; reset- and recovery time

this point a constant curve is visible (saturation point). Furthermore, I fitted a function to estimate the point where 50% and 90% of the full efficiency is reached. Moreover, the raise of the function for the dividing line between dead and reset time is calculated by the point where the gradient of the fitting function is not zero any more. The calculated points are visualized in fig: 4.7 and the final recovery time is  $\tau_{rec}^{90\%} = (21.21 \pm 0.34)ns$ , where  $\tau_d = (14.13 \pm 0.14)ns$  is the dead time and  $\tau_r = (7.08 \pm 0.36)ns$  the reset time. Moreover, the time the detector is back at efficiency of  $\eta_{sde} = 50\%$  is  $\tau_{rec}^{50\%} = (18.21 \pm 0.24)ns$ .

### 4.3 Efficiency

There are three types of efficiencies that describe independent loss processes in single photon detection. An efficiency can be equated with the probability that a quantum mechanically process under consideration will occur.

These three efficiencies are the coupling efficiency ( $\eta_K$ ), the absorption efficiency ( $\eta_A$ ) and the registration efficiency ( $\eta_R$ ). The graph 4.8 shows schematically where the different loss in the detection process appears. When a photon is sent to a detector via an optical fibre, not all photons can be coupled into the fibre. The probability of coupling is called the *coupling efficiency*. When photons hit the detector, there is always a probability that the photon will not be absorbed by the detector. This is due to material and symmetry properties. This is described by the *absorption efficiency*. Finally, there is always a probability that the photon will not be registered by the measuring electronics. This is expressed with the *Registration efficiency*.

In literature, these terms are summarized in two general efficiency terms: the device detection efficiency ( $\eta_{dde} = \eta_A \cdot \eta_R$ ) and the system efficiency ( $\eta_{sde} = \eta_A \cdot \eta_R \cdot \eta_K$ ) [4]. The device's efficiency  $\eta_{dde}$  corresponds to the efficiency of the device itself, when photons are sent to the detector in a free environment without any fibre coupling. In this way only the efficiency of the elements detecting photons are considered. The system detection efficiency  $\eta_{sde}$  takes the coupling losses to the optical fibre into account. This is the case if the detector is connected to a fibre, as the device properties or the experiment does not allow photon detection in a free environment.

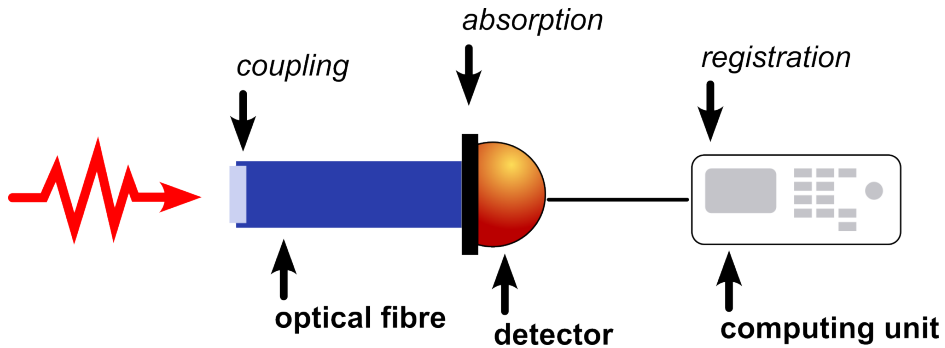


Figure 4.8: Sketch of the components in the detector setup where photonlosses appear and consequently a probability ( $\eta_K$ ,  $\eta_A$  or  $\eta_R$ ) has to be considered.

## Measurement and results

**DISCLAIMER: ALL THE RESULTS AND METHODS ARE NOT FINALIZED AND WILL BE ADAPTED, IF METHOD IS AGREED**

In the given setup, only the system detection efficiency  $c$  is measured, because the detector is already prebuild with a fixed coupling to a fibre. This internal fibre is connected to a fibre to fibre port (FC/PC to FC/PC). Through this one, one can connect the detector with an external fibre and send photons from the experiment to the detector.

The system detection efficiency  $\eta_{sde}$  is measured in different ways, each pointing out a different dependency. Each measurement was done in the setup explained in part 3. In addition, the order of the measurements is a relevant factor, as the conclusions drawn for one measurement influence the preceding measurements.

In conclusion, it is first necessary to align the polarization of the laser light with the slow axis of the fibre connected to the output port of the detector. Along the manual the coupled light needs to polarized along the slow axis of the fibre [manual\_single\_quantum\_snspd]. This is explained by the technical fact that only the slow axis of the fibre is coupled to the output port of the detector. The reason for this preselection of polarization is the related maximum  $\eta_A$ , explained in part 2.

By adjusting the laser beam linear with a quarter-wave plate first and rotating the half-wave plate in 10 degree steps afterwards, the polarization axis was rotated. With this, it was possible to find the angle configuration were the maximum of light was coupled to the slow axis of the fibre. This is important since measuring subsequent efficiency measurements aligned to a different axis would put a systematic downshift on the true efficiency of the detector.

In the figures 4.9(b) the count rate and the resulting system detection efficiencies are depicted. For preceding measurements the polarization was aligned to an angle, where a maximum of  $\eta_{sde} = 81.652 \pm 10.872$  was reached.

In a second measurement the bias current und trigger voltage dependency was investigated. For this the bias current was swept from 0 to  $35\mu\text{A}$  in  $0.1\mu\text{A}$  steps and events within 200ms integration time were counted.

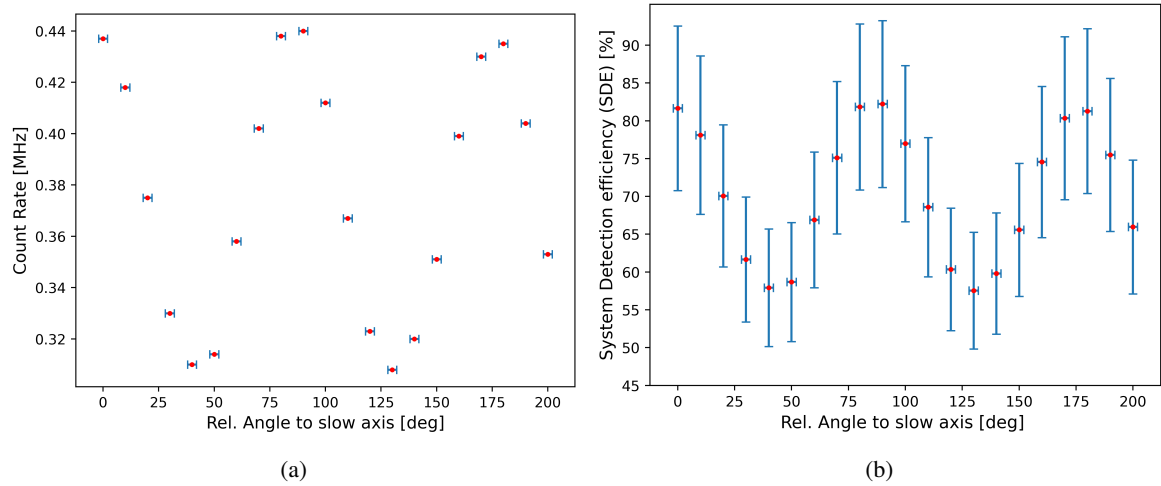


Figure 4.9: (a) Angle dependent countrate (b) Angle dependent system detection efficiency  $\eta_{\text{SDE}}$

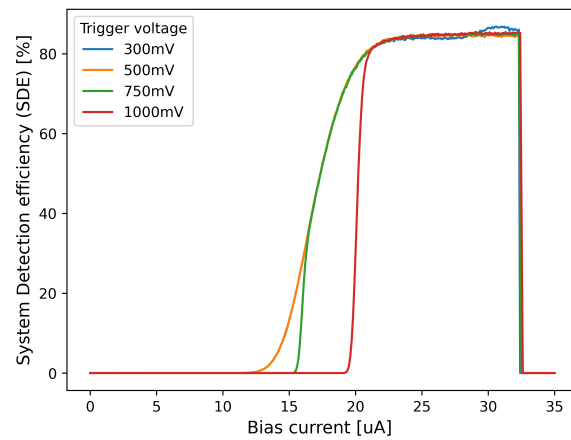


Figure 4.10: System detection efficiency for different bias currents and trigger voltages

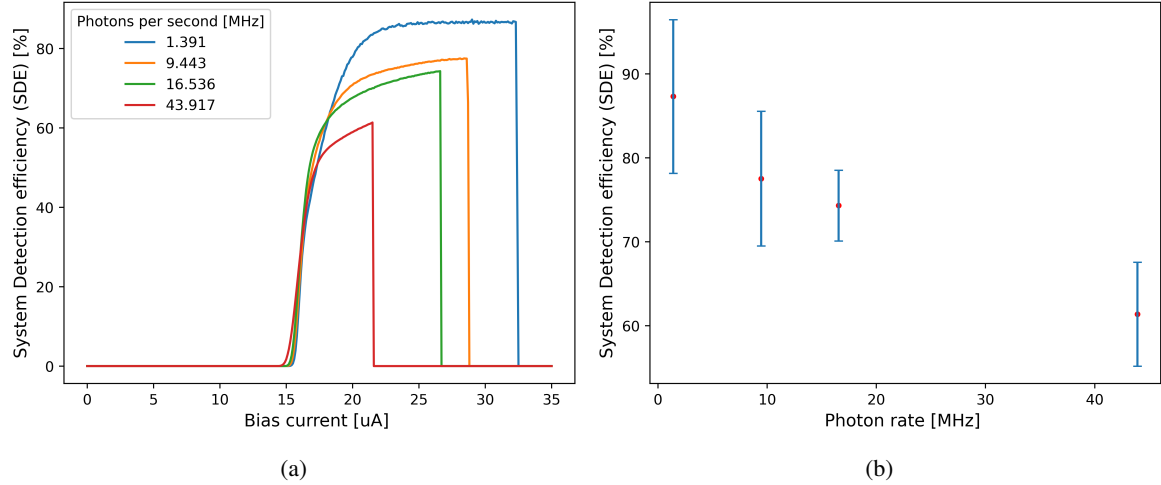


Figure 4.11: (a) Course of system detection efficiency for different bias current and count rates (b) Course of system detection efficiency for different count rates

In fig 4.10 one can see that at lower trigger voltage of 300mV the count rate oscillates a bit, which again corresponds likely to the increased dark count rates as explained in 4.6. Furthermore, one can see that for lower trigger voltages the detected counts for lower bias currents are higher. This is due to the consideration of lower voltage pulses in lower bias current regimes if the trigger voltage is low. Hence, with a lower trigger voltage one can count already signals, however, with a very low system detection efficiency  $\eta_{\text{sde}}$ . Another behaviour is the saturation, which is reached by each trigger voltage configuration at around  $I_{\text{Bias}} \approx 20\mu\text{A}$ . Here the maximum count rate is reached and the efficiency course continues constant without any gradient. At the end at a bias current of  $I_{\text{Bias}} \approx 32\mu\text{A}$  the efficiency drops. This is because the critical current is reached. After this, along the [manual\_single\_quantum\_snsdpd], the detector stops sending countable analog signals, which corresponds to an efficiency of zero.

Finally, measurements for different count rates were done, to determine the bandwidth where the photons are detected with the highest efficiency. The count rates were varied by using different ND filters and was done by putting together different ND filter combinations in order to get different OD values and therefore different count rates. To avoid the oscillation of count rates near the critical current as seen by the blue course in fig 4.10 a trigger voltage of 750mV is used.

In fig 4.11(a) one can see that the system detection efficiency is decreasing with increasing count rates. Moreover, only for the measurement of 1.391MHz one gets a range of bias currents where the efficiency is constant. All the other measurements with higher count rates show a continues increase in  $\eta_{\text{sde}}$  up to the point the detector shut down. Furthermore, the shut-down happens earlier, when the count rate is higher. This dynamics follows from the fact that the detector is not able to recover in time, when the count rate is too high. Hence, the critical temperature is reached earlier, when the count rate is raising and the detections is shut down.

In fig 4.11(b) the maximum system detection efficiency for each count rate is shown. One see clearly a downward trend for raising count rates. Moreover, the measurement shows the saturating and therefore a maximal system detection efficiency of  $(87.308 \pm 9.159)\%$  for channel 1. This  $\eta_{\text{sde}}$  is reached at a count rate of  $1.391 \pm 0.32\text{MHz}$ .

## 4.4 Discussion

## **CHAPTER 5**

---

### **Conclusion and Outlook**

---

# APPENDIX A

---

## Appendix

---

### A.1 ND filter calibration

To calculate the OD value of the ND Filters, we first calculate the Transmission value:

$$T = \frac{P_{detected}}{P_{input}}$$

For the Error calculation we have to consider two error sources. Once the measurement uncertainty of the photodiode and the measurement uncertainty from reading the value from the Powermeter. Since the uncertainty from the photodiode is always 3% of the measured value, it does not contribute to the error, since the transmission is a division and this does not affect the overall relation. However, reading of the value from the powermeter provides always a different error because the last displayed order of magnitude of the displayed result on the powermeter fluctuates.

Its also important to mention that after each adjustment for the fiber coupling, it was not possible to get to the same initial value. Therefore, we always have different power values we compare, though the filtering process was done always with the same amount of light power. So we have to consider an error from the fiber coupling and optimization. For this our  $P_{input}$  value for the Transmission is in reality not the measured value we coupled in but the averaged value with an standard deviation as error. Also, this only applies for the first measurement method because we adjust there our fiber coupling. In the second measurement we have a stable  $P_{input}$

So for the transmission error we got:

$$\Delta T = \sqrt{\left(\frac{\Delta P_{detected}}{P_{input}}\right)^2 + \left(\frac{\Delta P_{input} P_{detected}}{P_{input}^2}\right)^2} \quad (\text{A.1})$$

Where.

$$\Delta P_{Input} = \sqrt{(P_{detected}^{Pow.meterreadoff})^2 + (P_{detected}^{STD,coupling})^2} \quad (\text{A.2})$$

And with the relation:  $OD = \log(\frac{1}{T})$  we can calculate the error for the OD:  $\Delta OD = \frac{\Delta T}{\ln(10) \cdot T}$

## Appendix A Appendix

---

Regarding the errors it is important to mention that the error of the photodiode is not relevant if we look at the error of the transmission rate because its the same for the measurement before and after the ND Filters.

In general the measurement error of the photodiode is about 3% of the measured value [Powermeter specs](#). This error I considered only in the calculation for the output power error:

Table with measurement values and results for Transmission value and OD Value

ID	Expected OD Value	Measured T Value	T Value Error Systematic	T Value Error stat	T Value Error	Mean OD Value	OD Value Error
TP03337667	1.00	1,43E-01	67,697E-4	3,223E-03	7,50E-03	0,844	0,023
TP03337667 (2)	1.00	1,47E-01	50,474E-04	3,073E-03	5,91E-03	0,832	0,017
TP03366490	3.00	8,26E-03	32,418E-05	1,882E-04	3,75E-04	2,083	0,020
TP03366490 (2)	3.00	7,93E-03	52,291E-05	1,744E-04	5,51E-04	2,101	0,030
TP03275234	4.00	1,00E-03	5,318E-05	4,381E-05	6,89E-05	2,999	0,030
TP03312353	4.00	1,04E-03	7,142E-05	4,312E-05	8,34E-05	2,983	0,035
TP03271009	4.00	1,02E-03	4,842E-05	4,432E-05	6,56E-05	2,991	0,028
TP03275234 (2)	4.00	1,03E-03	6,566E-05	4,303E-05	7,85E-05	2,986	0,033
TP03324728	5.00	1,80E-04	9,945E-06	3,843E-05	3,96E-05	3,744	0,095
TP03287742	5.00	1,78E-04	4,196E-06	3,731E-05	3,75E-05	3,749	0,092
TP03348187 (2)	5.00	1,82E-04	4,506E-06	3,921E-05	3,95E-05	3,739	0,094
TP03348187	5.00	1,82E-04	5,792E-06	3,862E-05	3,91E-05	3,739	0,093

Calculating the error for stacked ND filters. The Error from

$$P_{input} = P_{Input}^{initial} \cdot 10^{-OD} \quad (\text{A.3})$$

constructed out of the uncertainty of the Photodiode  $\Delta P_{Input}^{initial} = 0.03 \cdot P_{Input}^{initial}$  and the error of the ND Filters

$$\Rightarrow \Delta P_{input} = \sqrt{(\Delta P_{Input}^{initial} \cdot 10^{-OD})^2 + (P_{Input}^{initial} \cdot \log(10) \cdot \Delta OD)^2} \quad (\text{A.4})$$

The Error  $\Delta P_{detected}$  is reformed to a rate only in the order of a few hundred Herz and is neglectable compared to the  $\Delta P_{input}$ .

## A.2 Recovery time measurements

### A.2.1 Recovery time measurements - Oscillating bias current

**Method 1 and 2 combined:** In both tables above one can see that the second method has slightly higher values. This indicates a systematic error we dont know. Till now, we only considered statistical errors. Now if we want to calculate the true value we have to consider the systematic error as well. Here we determine the systematic error as half of the difference between the values from method one and method two  $\Delta T_{syst} = \frac{T_{meth_2} - T_{meth_1}}{2}$ . So the final transmission error of the combined measurements is:  $\Delta T = \sqrt{\Delta T_{stat}^2 + \Delta T_{syst}^2}$

In the appendix you usually include extra information that should be documented in your thesis, but not interrupt the flow.

---

# Bibliography

---

- [1] G. A. Steudle et al.,  
*Measuring the quantum nature of light with a single source and a single detector*,  
Physical review. A, Atomic, molecular, and optical physics/Physical review, A, Atomic,  
molecular, and optical physics **86** (2012),  
URL: <https://doi.org/10.1103/physreva.86.053814> (cit. on p. 2).
- [2] singlequantum.com, *Superconducting Nanowire Single Photon Detectors Operation principle*,  
<https://singlequantum.com/wp-content/uploads/2023/06/Single-Quantum-Operation-Principle-print.pdf>, Accessed: 2023-06, n.d. (Cit. on p. 3).
- [3] Single Quantum, *Single Quantum SCSPCM Manual*, 2024 (cit. on pp. 6, 7).
- [4] C. M. Natarajan, M. G. Tanner and R. H. Hadfield,  
*Superconducting nanowire single-photon detectors: physics and applications*,  
Superconductor science and technology/Superconductor science technology **25** (2012) 063001,  
URL: <https://doi.org/10.1088/0953-2048/25/6/063001> (cit. on pp. 9, 15).
- [5] R. H. Hadfield, *Single-photon detectors for optical quantum information applications*,  
Nature photonics **3** (2009) 696, URL: <https://doi.org/10.1038/nphoton.2009.230>  
(cit. on p. 9).
- [6] Wikipedia contributors, *Signal-to-noise ratio*, 2024,  
URL: [https://en.wikipedia.org/wiki/Signal-to-noise\\_ratio](https://en.wikipedia.org/wiki/Signal-to-noise_ratio) (cit. on p. 9).
- [7] K. Shalm et al., *Single-Photon Detector Tutorial*, Computer Scientist QCRYPT,  
National Institute of Standards and Technology, 2013, URL:  
<https://qcrypt.github.io/2013.qcrypt.net/contributions/Shalm-slides.pdf>  
(cit. on p. 12).
- [8] C. Autebert et al.,  
*Direct measurement of the recovery time of superconducting nanowire single-photon detectors*,  
Journal of applied physics **128** (2020), URL: <https://doi.org/10.1063/5.0007976>  
(cit. on p. 12).
- [9] S. Miki, M. Yabuno, T. Yamashita and H. Terai, *Stable, high-performance operation of a fiber-coupled superconducting nanowire avalanche photon detector*,  
Optics express **25** (2017) 6796, URL: <https://doi.org/10.1364/oe.25.006796>  
(cit. on p. 12).